Beam Test of CCDs for Vertex detectors of JLC

SHIRASAKI Yasuhiro

August 27, 1999

1 Introduction

The standard model of elementary particle physics has been verified with many experiments in these 30 years. The last quark so-called "top" was found by the Fermi laboratory experiment of the year 1994 in U.S.A with the accelerator TeVatron.

The Joint Linear Collider (hereafter JLC) is in the planning stage as linear electron-positron collider of the next generation, for the energy frontiers of elementary particle physics. The JLC is planned to generate any heavy particles, like a higgs or super symmetry particles, to verify the standard model with the above TeV total energy of e^+e^-. It is very hard to reconstruct tracks decayed from such short life-time particles. Therefore vertex detectors are necessary to determine the decay points of $b/\bar{b}, c/\bar{c}$ with high spatial resolution.

For the advanced detection of decay points, CCD is powerful candidate for vertex tracker in these days. Recent semiconductor processing technology improvement achieved to manufacture the high resolution detectors. The advantage of CCD is unambiguous reconstruction capability, less occupancy and less multiple scattering, when compared with silicon strip detectors.

As a precedent for an application of CCD vertex detector, SLAC Large Detector experiment has been carried out successfully. In the experiment they used the CCDs at near 180K. The thermal shrink rate difference between CCD and backing structures occur complex spatial distortion at such low temperature. It made some measurement errors in charged particle tracking. Cooling structures also caused more multiple scattering and lower resolution.

On the other hand, we will simplify cooling system and operate CCDs in near root temperature to reduce distortions of detectors and multiple scattering in our plan.

1.1 Measurement of spatial resolution

In the past experiments, we operated the full frame type CCD on the market in the so-called MPP mode at near the room temperature and measured S/N

ratio with ^{55}Fe 5.9 KeV X-ray source. It achieved sufficient S/N.

We measured incoming angle dependencies of spatial resolution for 3 kinds of CCDs in this study.

2 Experimental setup

The CCDs are exposed to π particles extracted from 12 GeV KEK-PS in T1 line from Jun. 15 to 22 in 1999.

2.1 Sensors

Two kinds of S5466 manufactured by Hamamatsu photonics and CCD02-06 by EEV are tested in this study. One S5466 has 10 μm of epitaxial layer, the another has 50 μm of it. (Table1)

CCD	HPK S5466		EEV
	(10um)	(50um)	CCD02-06
Effective area	512 × 512	←	385 × 578
Pixel Pitch	24 μm	←	22 μm
Chip size	12.288^2 mm^2	←	8.47 × 12.716 mm^2
Epitaxial Layer	10 μm	50 μm	20 μm
Amp. Sensitivity	2.0μV/e	←	1.0μV/e

Table 1: Specifications of CCDs

Each of CCD sensor is mounted upon the Al_2O_3 body.

2.2 Setup

Three reference sensors and one target sensor are kept in a constant temperature box at several near room temperatures. In this study, data taken at -15C° is used. Coincidence of two monitoring plastic scintillaters placed in front of target sensors are used to count passing charged particles (Fig1).

The special chip which have no Al_2O_3 behind a sensor is used as second layer (CCD1) to avoid multiple Coulomb scattering effect. The sensors of CCD0 and CCD1 faces downstream side, that of CCD2 and CCD3 faces upstream side for the same reason. Therefore multiple Coulomb scattering caused with Al_2O_3 are negligible.

The detector is exposed to 2.0, 1.0, 0.7 and 0.5 GeV/c minimum ionized particles (MIPs, π^-). The angles of beam incidence to sensors are kept to 0°, 45° and 60° (Fig19).

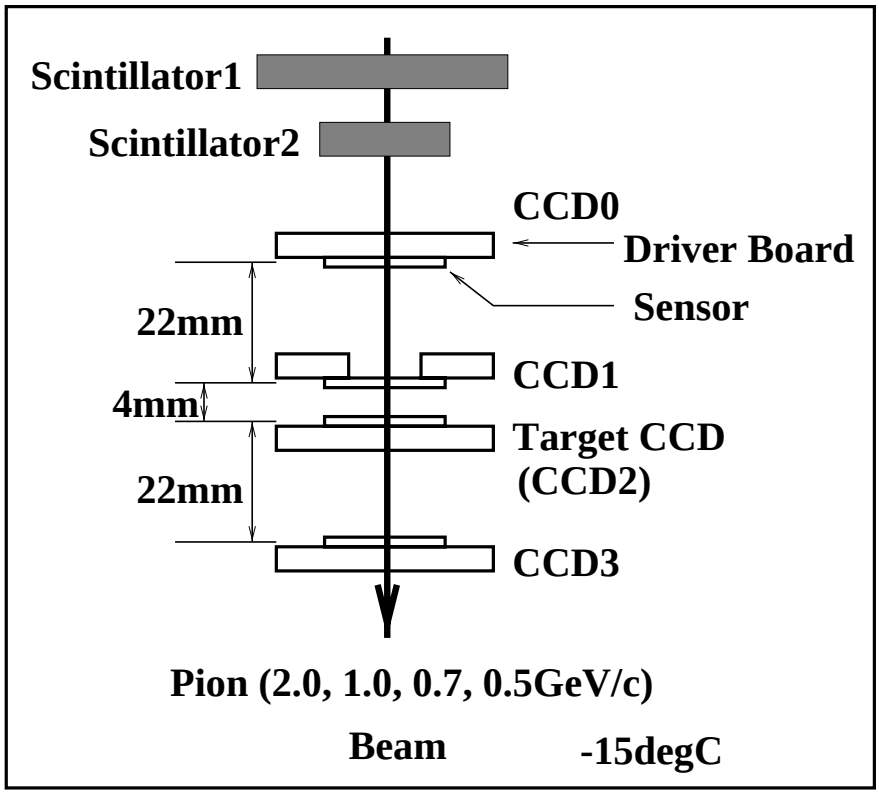

Figure 1: Setup

3 Track positions detection of charged particles

3.1 Clustering

Incoming charged particles tends to spread a charge deposit to neighbor pixels of hit pixel. For the measurement of the total charge deposit, it is necessary to collect charge informations from adjacent pixels. The ratio measurement of charge sharing among adjacent pixels may improve the precision of the track position detection to sub-pixel size. Therefore we study about the clustering method described as follows.

3.2 The Center of gravity

First, we search the pixel which has an ADC count discriminate over the threshold. The threshold is determined to reduce bogus fits caused by noises lower than 5% with dark frame. We call the pixel found with such threshold which has locally highest ADC count "local peak".

Consider extending the $n \times m$ rectangular region which includes the local

peak pixel. We call the region "cluster". Increase n or m to make the largest charge ADC count sum of $n \times m$ region. Stop extending the region when the increase of sum of ADC count is less than a δQ. If larger ADC count then first local peak is found in extending the region, cancel the first local peak. Fig2 shows the charge distribution of such clusters.

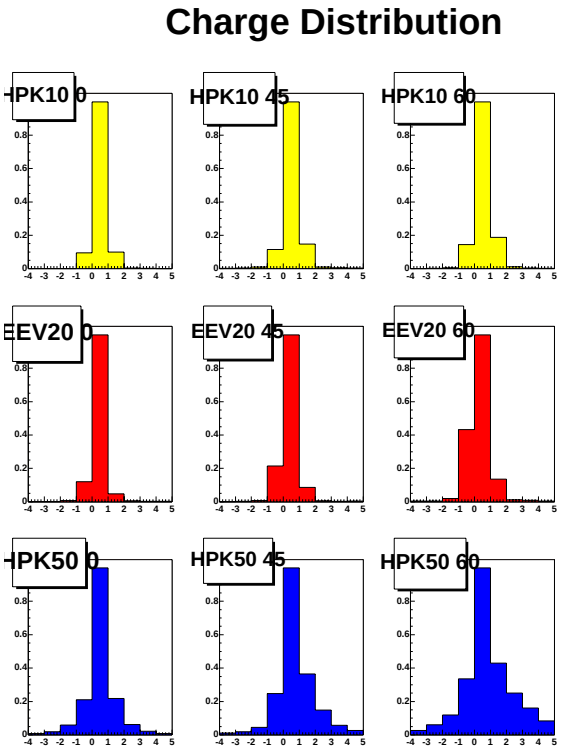

Figure 2: Charge distribution of cluster $(0°, 45°, 60°)$

It shows that thicker the epitaxial layer is (HPK10, EEV20, HPK50), The size of cluster grows. When the incoming angle is $45°, 60°$, charge distribution becomes asymmetry.

For the cluster region found with the method described as above, calculate the center of charge X:

$$X = \frac{\sum Q_i X_i}{\sum Q_i}$$

Consider X as the position where the charged particle hit.

We compare the δQ of 0.02, 0.05 and 0.08. When the size of cluster is determined as 1×1, consider the center of pixel as the hit position.

3.3 correction

With the finding method of the hit position described as above, the projection of positions to X axis shows a periodical distribution which has the same size of CCD pixels (Fig 3).

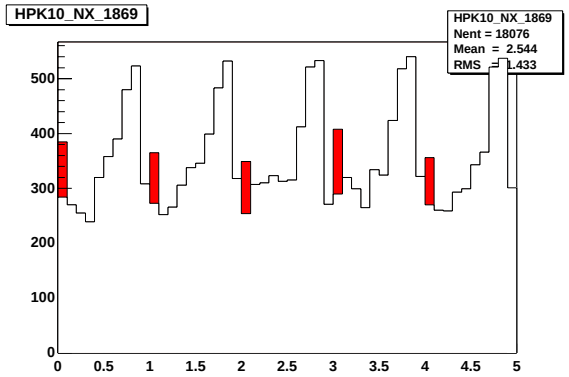

Figure 3: The center of clusters with linear sum. colored has a cluster size of 1×1

Since incoming beam has no periodical density which size is same to the pixel size and it should has uniformity, potential wall of CCD prevents to diffuse the generated charge and might cause the periodical distribution in the fig 3.

Therefore assuming the uniform incoming particles, we correct the position X calculated with the linear charge sum. It may improve the precision of the position. Assuming the uniformity ($\frac{dN}{dX}$ =constant), we do the correction:

$$\begin{aligned} r &= [X+1] - X \\ \delta(r) &= \frac{1}{N}\int_0^r \frac{dN}{dx}dx \\ X' &= X - r + \delta(r) \end{aligned}$$

Fig4 shows rough uniformity of corrected positions. Since colored pixels in the histogram which has 1×1 cluster size is never affected with the correction, the histogram has small peaks of such pixels.

3.4 Ratio Location Mapping

Choose the maximum ADC count sum of four 2×2 square regions in 3×3 region which has a local peak at its center. We assume it is the cluster candidate.

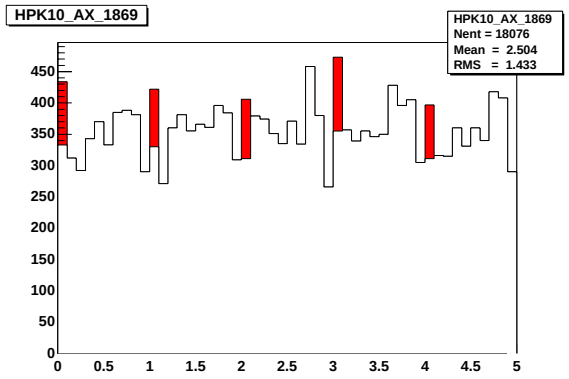

Figure 4: The center of clusters with linear sum and correction. colored has a cluster size of 1×1

With the ADC count ratio of local peak and adjacent pixel R_x and uniformity of incoming particles,

$$\frac{dN}{dx} = \text{const}, R_x = \frac{C_{\text{next}}}{C_{\text{peak}}}$$

follows

$$\begin{aligned} X(\log(R)) &= \frac{0.5}{N} \int_{-\infty}^{\log(R)} \frac{dN}{d\log(r)} d\log(r) \\ &= \sum_{n=0}^{\infty} a_n \log^n(R) \end{aligned}$$

determine the expand coefficients with real data. Using the expanded function, we calculated positions of each cluster (Fig 5). We used approximated function 5th order (Fig 6). For example the function for HPK10μm, 60°

$$\begin{aligned} X(r) &= (0.64 \pm 0.08) + (0.51 \pm 0.10)r - (0.13 \pm 0.15)r^2 - (0.14 \pm 0.09)r^3 \\ &\quad +(0.03 \pm 0.06)r^4 + (0.02 \pm 0.03)r^5 \end{aligned}$$

$(r = logR)$.

Expand coefficients has incidence angle dependency. The figure shows that charge sharing is not uniformly, when the incidence angle is not vertical.

4 Alignment

4.1 Residual

Determine the spatial resolutions with CCD0, CCD1 and CCD2. CCD3 is used to check the bogus tracks.

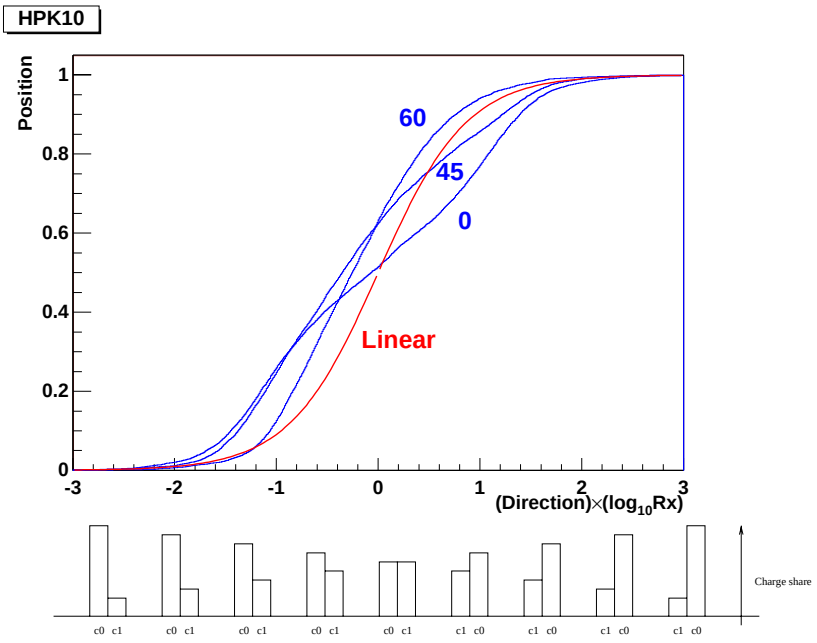

Figure 5: RLM Mapping function

Find the intersection point for linear extension of cluster on the CCD0 to that on the CCD1 and CCD2 surface. Define the difference between that intersection point and clusters on CCD2 as residual (Fig 7).

If CCD0, CCD1 and CCD2 are parallel to each other, residual is showed with the distance between CCD0 and CCD1 (d1) and that of CCD1 and CCD2 (d2):

$$\text{Residual} = x3 - \left\{ x2 + \frac{d2}{d1}(x2 - x1) \right\}$$

We used rectangular coordinates and set the center of CCD1 as the origin (Fig 7).

4.2 Rough alignment

First, we assume all the detectors are parallel to align roughly. We plot the relative position of clusters on CCDn (n = 0, 2, 3) to the cluster positions on CCD1 and find the peaks determine large gap in X-Y plane:

$$\delta X_i = X_i - X_1 (i = 0, 2, 3)$$

After that, determine Z directional displacement with:

$$Z = \frac{X_2 - X_1}{X_1 - X_0}$$

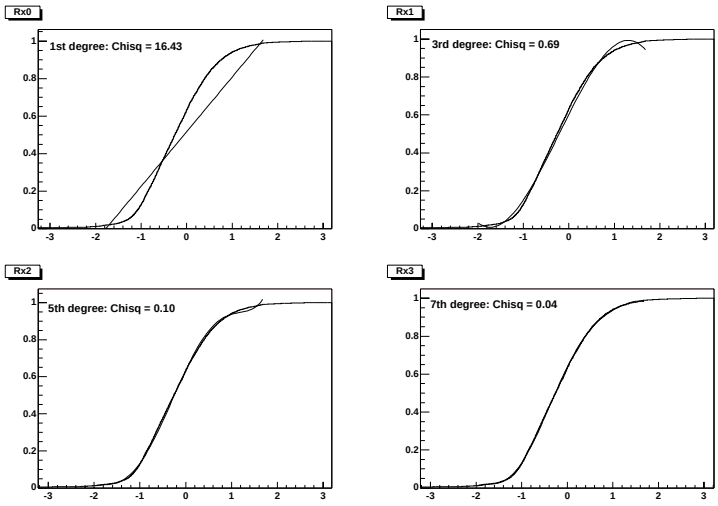

Figure 6: RLM Mapping approximation

Determine the rotation on the X-Y plane with the correlations of $dx - Y$ and $dy - X$.

4.3 Track Selection

With the rough alignment described as above, we find particle track candidates in certain reliability. Since the distance ratio of CCD1 - CCD2 and CCD1 - CCD3 is about 1:5, We assume the track which has the smaller residual on CCD3 than five times of residual extent on CCD2 (σ) as candidates (Fig 8).

4.4 Residual Minimization

When we split the track candidates to the 4×4 region groups with cluster position on the CCD1 and plotted residuals. The histogram in the Fig 9 shows an rule based mean value transition.

The tilt of CCD planes against reference CCD might caused such transitions. We assume CCD0 and CCD2 has rotations against CCD1 and minimize square sum of residuals with the parameters as follows (Fig 7):

$$\begin{pmatrix} x' \\ y' \\ z' \end{pmatrix} = (\theta)\,(\phi)\,(\xi) \begin{pmatrix} x \\ y \\ 0 \end{pmatrix}$$

Table 2 shows typical minimized parameters.

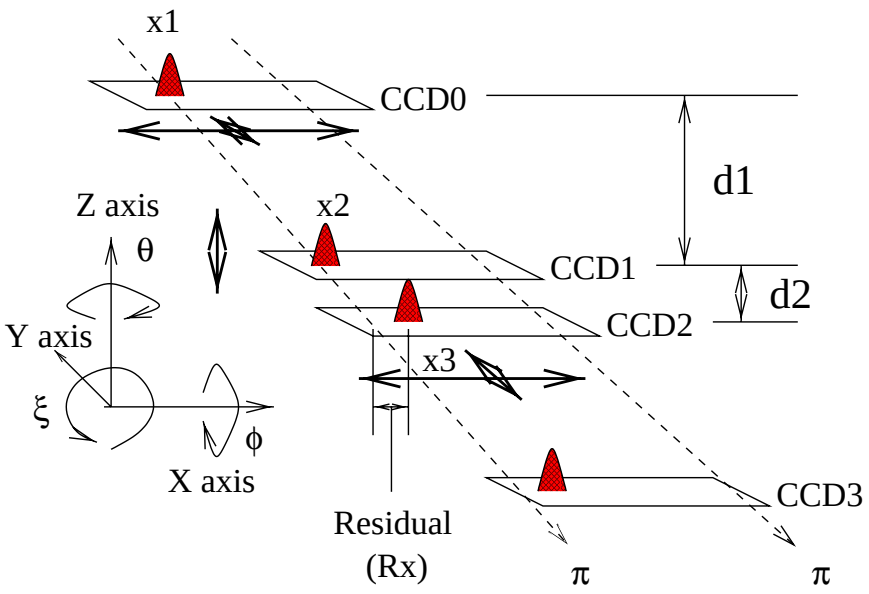

Figure 7: Residual and coordinates

Parameters	Value	Parameter	Value
θ_0	0.002 ± 0.005	θ_2	0.000 ± 0.001
ϕ_0	-0.010 ± 0.006	ϕ_2	0.002 ± 0.001
ξ_0	-0.010 ± 0.005	ξ_2	-0.006 ± 0.001
δX_1	-0.094 ± 0.011	δY_1	-0.002 ± 0.011

Table 2: Residual typical minimization parameters(HPK50, 60°)

5 Analysis

5.1 Momentum dependency of spatial resolution

For the each momentum 2 - 0.5 GeV/c, spatial resolution is combination of intrinsic spatial resolution $\sigma_{\text{intrinsic}}$ and multiple scattering $\sigma_{\text{scattering}}$. The measured residual distribution σ_{residual} is written as:

$$\sigma_{\text{residual}} = \sqrt{\sigma^2_{\text{intrinsic}} + \sigma^2_{\text{scattering}}}$$

$\sigma_{\text{scattering}}$ is in inverse proportion to momentum of the particles.

$$\sigma_{\text{scattering}} \propto \frac{1}{p}$$

Therefore fitting the function to the spatial resolutions for each momentum and extrapolating the intrinsic resolutions with $p \to \infty$ (Fig 10).

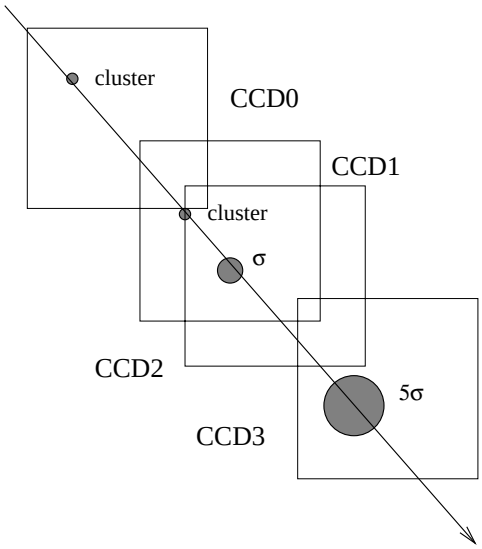

Figure 8: assume the track which has the smaller residual on CCD3 than five times of residual extent on CCD2 (σ) as candidates

σ_{residual} is combination of all the resolutions for each CCD and showed:

$$\sigma^2_{\text{residual}} = \sigma^2_{\text{CCD2}} + (1+Z)^2\sigma^2_{\text{CCD1}} + Z^2\sigma^2_{\text{CCD0}}$$

Here Z is $\frac{d2}{d1}$. When we used HPK10 target CCD, we assumed:

$$\sigma_{\text{CCD0}} = \sigma_{\text{CCD1}} = \sigma_{\text{CCD2}}$$

It worked out the intrinsic resolution for each CCD.

5.2 Intrinsic resolution

Table 3, 4, 5, Fig 13 show intrinsic resolutions for each incoming angle and CCDs.

CCD	Resolution (μm)	
	Center Of Mass	RLM
HPK 10	3.87 ± 0.05	2.98 ± 0.05
HPK 50	2.35 ± 0.10	2.26 ± 0.19
EEV 20	3.90 ± 0.12	2.73 ± 0.30

Table 3: 0°

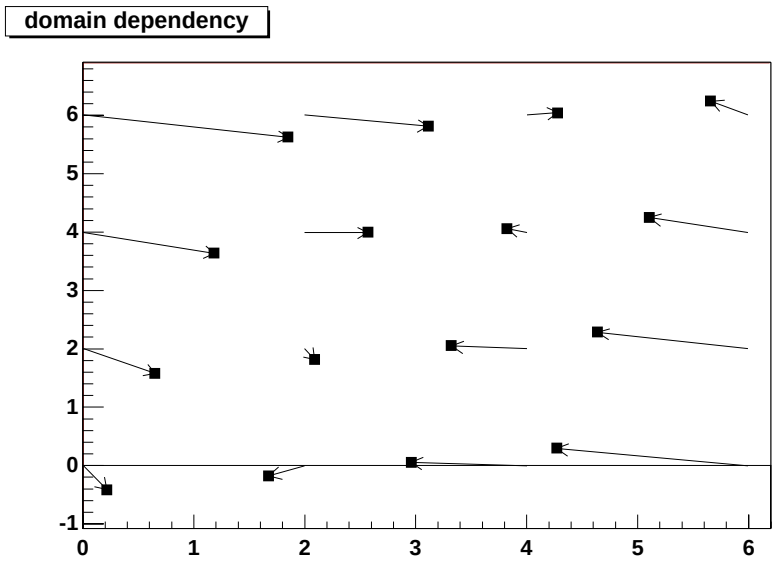

Figure 9: Cluster position on CCD1 dependency of residual. unit is [pixel] and 1 pixel = 24μm

Normal incident

When the incident particles on CCD is perpendicular, the results with the RLM method is better than that with the COM method for HPK10 and EEV.

45 degree incident

With 45 degree incident, HPK10 and EEV resulted in good resolution. Comparing the COM and the RLM method, the former is better with HPK50

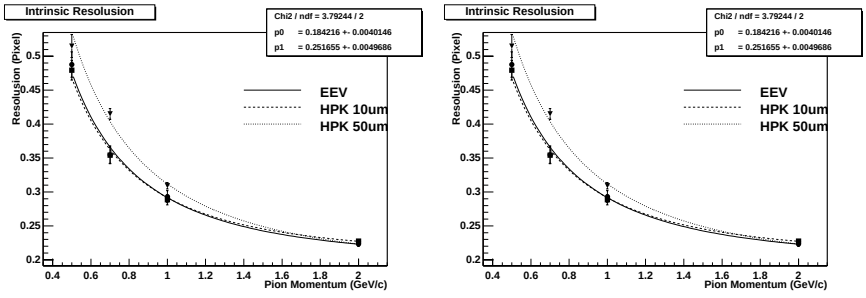

Figure 10: Momentum dependency of spatial resolution (0°)

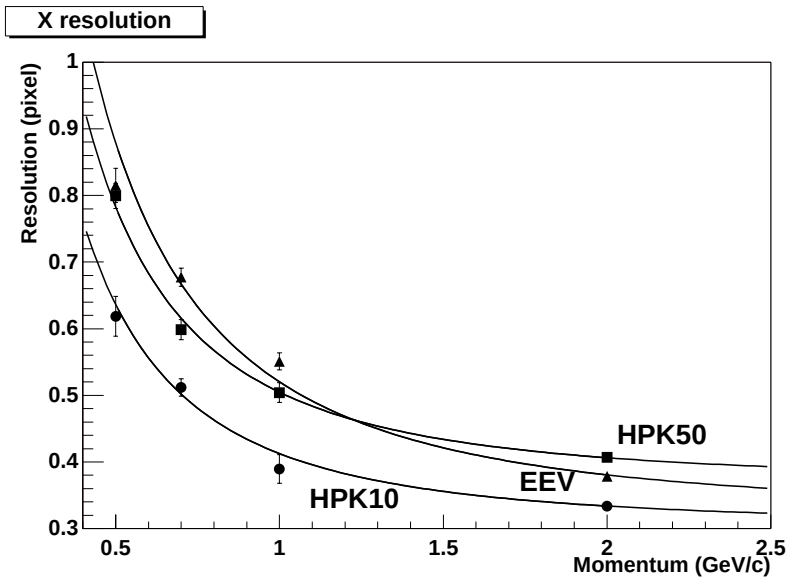

Figure 11: Momentum dependency of spatial resolution (45°)

CCD	Direction	COM	COM(Mod)	RLM
HPK 10	X	4.65 ± 0.06	4.53 ± 0.06	2.86 ± 0.10
	Y	4.72 ± 0.05	4.30 ± 0.06	2.58 ± 0.07
HPK 50	X	6.15 ± 0.15	6.16 ± 0.14	6.97 ± 0.16
	Y	3.31 ± 0.11	3.20 ± 0.12	3.68 ± 0.12
EEV 20	X	3.98 ± 0.13	3.73 ± 0.13	3.62 ± 0.17
	Y	3.80 ± 0.10	3.41 ± 0.11	3.14 ± 0.12

Table 4: 45°

which has thicker, and the later is better with HPK10 and EEV which has thinner epitaxial layer. Corrections for COM method improved in some cases, but it seems same in the errors.

The very good resolution for the RLM method with HPK10 might make the resolutions for HPK50 and EEV worse. (Fig 14, 15, 16)

60 degree incident

With 60 degree incident HPK10 got good results. The dependency of spatial resolution for X position on the CCD described following section and insufficient samples with low energy beam made it difficult to discuss the merits of three CCDs.

In the all cases COM method was better than RLM method.

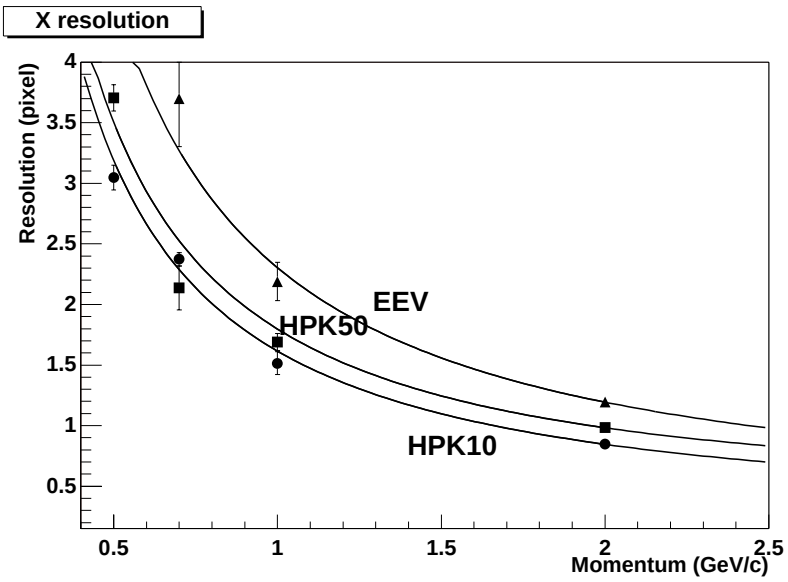

Figure 12: Momentum dependency of spatial resolution (60°)

CCD	Direction	COM	COM(Mod)	RLM
HPK 10	X	5.60 ± 0.92	4.33 ± 0.98	7.27 ± 0.85
	Y	5.40 ± 0.34	5.34 ± 0.36	4.61 ± 0.30
HPK 50	X	9.58 ± 1.71	9.47 ± 1.89	16.97 ± 1.92
	Y	5.12 ± 0.72	4.79 ± 0.71	3.61 ± 0.83
EEV 20	X	5.85 ± 3.52	2.47 ± 5.27	5.67 ± 7.51
	Y	6.68 ± 0.91	6.76 ± 1.09	3.48 ± 1.12

Table 5: 60°

5.3 The center of mass method and the ratio location mapping method

Dynamic determination of the cluster size for the COM method with its charge distribution got good result than the RLM method which uses only 2×2 region when the charge extend more than three pixels. HPK50 with 45 degree incident and all the CCDs with 60 degree incident is in such case.

On the other hand, the RLM method is better because it is sensitive for fine charge ratio change when most charge is stay in the 2×2 region.

5.4 Cluster threshold dependency of spatial resolution

The spatial resolutions with the COM method may depend on the clustering threshold. The threshold determines how extent the clusters. We stopped

for extension when the total charge change for extension is (δQ) smaller than 2% as mentioned above.

We changed the threshold 2%, 5%, and 8% and got the following result. Table 6 and figure 17 shows the result. 5% of threshold got the best result and 8% of it is worse. Anyway the change of the resolution is not so large.

δQ	X [pixel]	Y [pixel]
2%	0.35 ± 0.01	0.27 ± 0.01
5%	0.33 ± 0.01	0.23 ± 0.01
8%	0.37 ± 0.01	0.30 ± 0.01

Table 6: δQ dependency of spatial resolutions (HPK50, 45degree)

5.5 The track passing position dependency

In this experiment, spatial resolution had a position dependency for X direction of CCD for each momentum. Figure 18 shows typical example. a quarter of left region is worse.

The reason might that CCD has the size of $12mm^2$ but the hole in the ceramics package is $10mm^2$. The incident particles passing out of hole might be scattered with the ceramics package.(Fig19).

Therefore we checked the intrinsic resolutions without the tracks which pass the left half of the CCD (Fig 20, Table 7).

CCD	direction	COM	COM (w/ correction)	RLM
HPK 10	X	4.73 ± 0.08	4.56 ± 0.10	3.30 ± 0.06
	Y	4.64 ± 0.07	4.53 ± 0.09	2.57 ± 0.05
HPK 50	X	6.56 ± 0.17	6.68 ± 0.18	6.92 ± 0.14
	Y	4.44 ± 0.14	4.39 ± 0.16	3.79 ± 0.10
EEV 20	X	4.72 ± 0.18	5.05 ± 0.19	4.37 ± 0.16
	Y	5.70 ± 0.15	4.87 ± 0.18	3.34 ± 0.13

Table 7: 45° (left half of CCD, HPK10

The result shows that the intrinsic resolutions are not different. With the EEV, as it has three fourth size of HPK, the exclusion of right half caused the lack of samples.

Figure 21 shows residual distribution for HPK50 and 60 degree incident with left half, right half or all the tracks. Figure 22 shows the case freeing the center of rotation for CCD0 and CCD2.

In any case the residual distribution did not change.

5.6 Check

Figure 23 shows the X direction dependency of residual even if we did not consider any tilt of CCDs.

6 Summary

Measurement of spatial resolution for CCD manufactured by Hamamatsu and EEV with $0°, 45°, 60°$ incident π^- was carried out.

Hamamatsu 10μm had good spatial resolution ($< 6\mu m$) with incident particles at an angle of $45°, 60°$.

In this experiment, with incident particles at an angle of $45°, 60°$, tracks had different thickness of passing matter which depends where the track passed. The problem was clear with Hamamatsu 50μm and EEV 20μm.

With normal incident particles and small charge diffusion, the ratio location mapping method was better than the center of mass method. Because the former is sensitive to a little charge distribution change. On the other hand, with the particles at an angle of $45°, 60°$ and large diffusion, CCDs which has thick epitaxial layer could not get good result with the RLM method which only uses information from center area of clusters. the COM method was better than the RLM method in such cases.

We should measure more precise spatial resolution with the better experimental setup in the future.

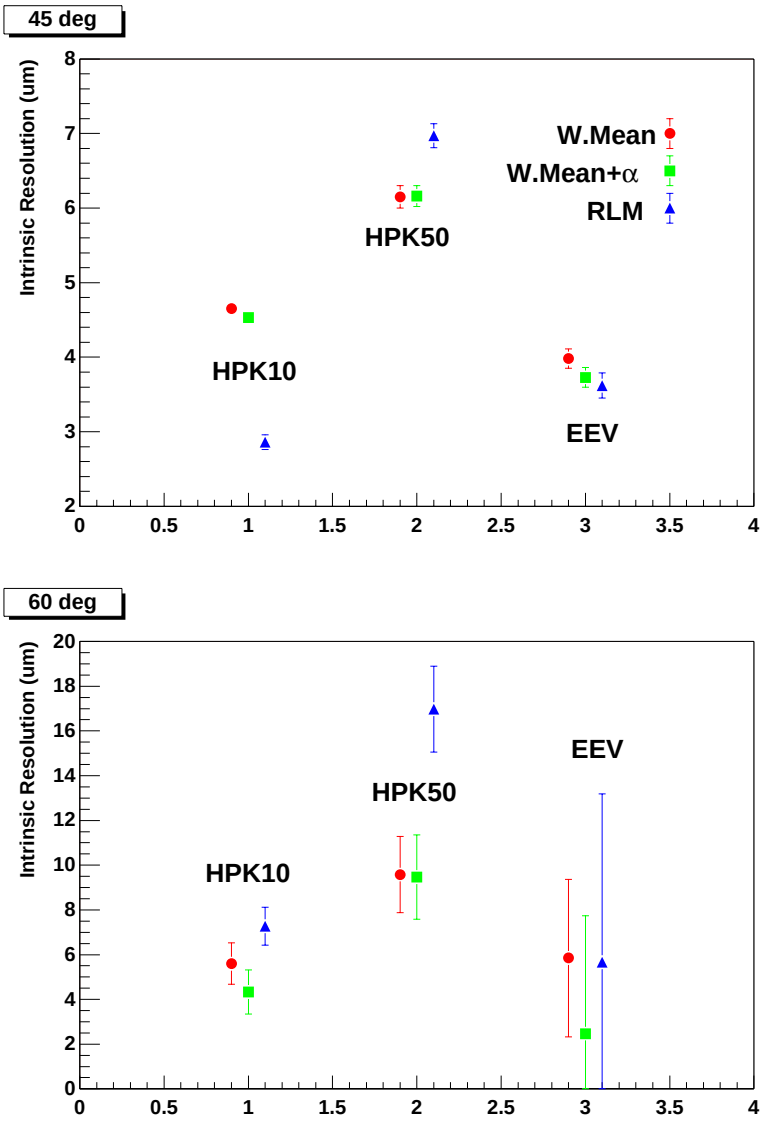

Figure 13: Intrinsic resolution for each incoming angle

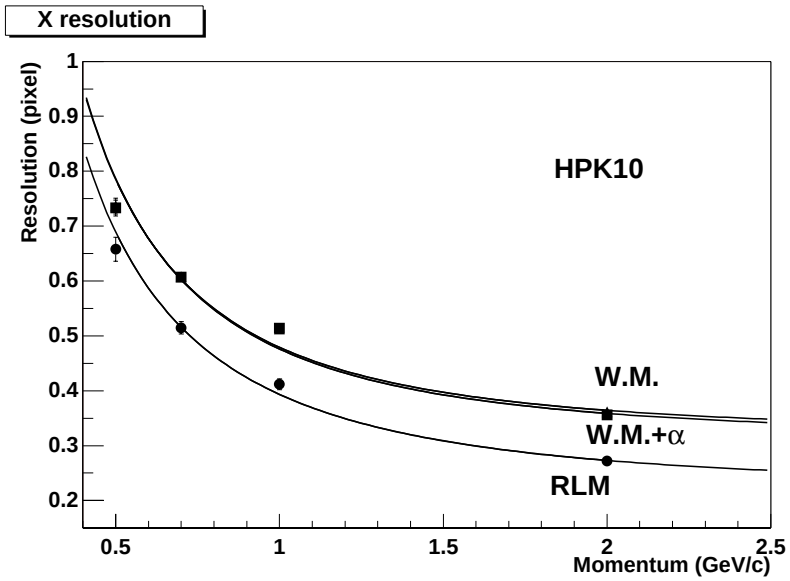

Figure 14: 45 degree incident HPK10μm

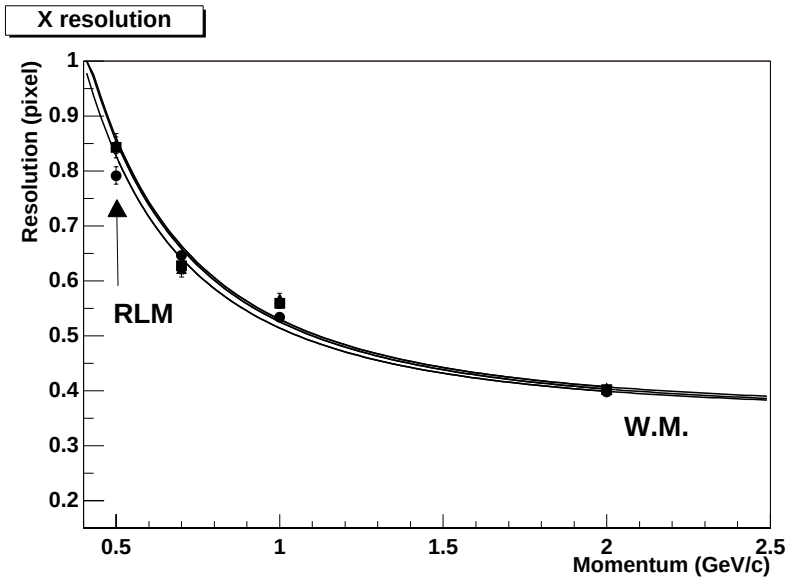

Figure 15: 45 degree incident HPK50μm

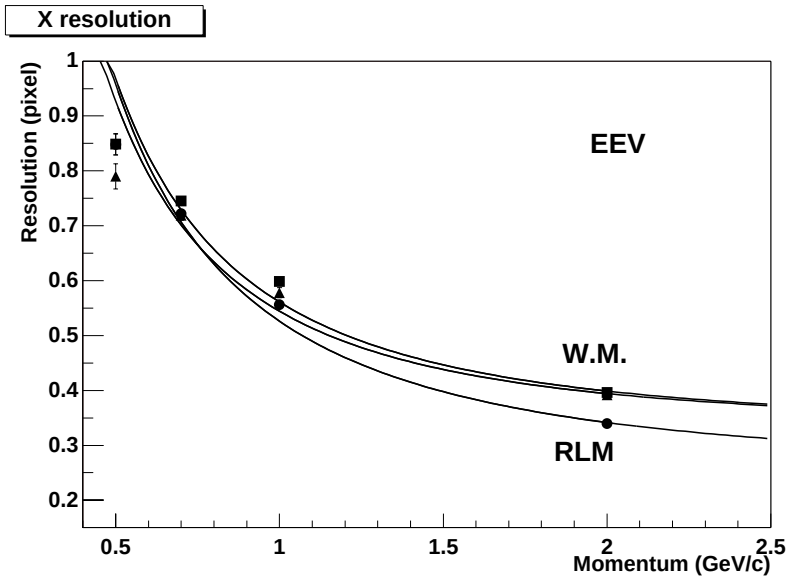

Figure 16: 45 degree incident EEV20μm

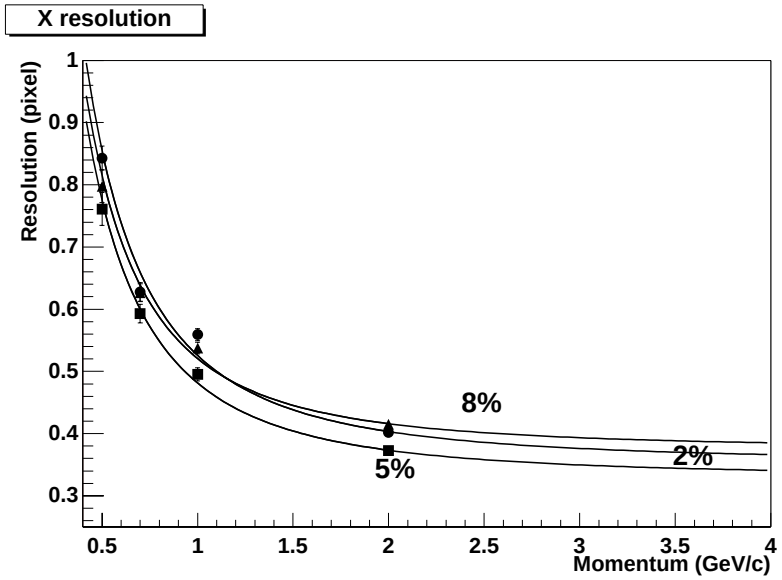

Figure 17: δQ dependency of spatial resolutions (COM)

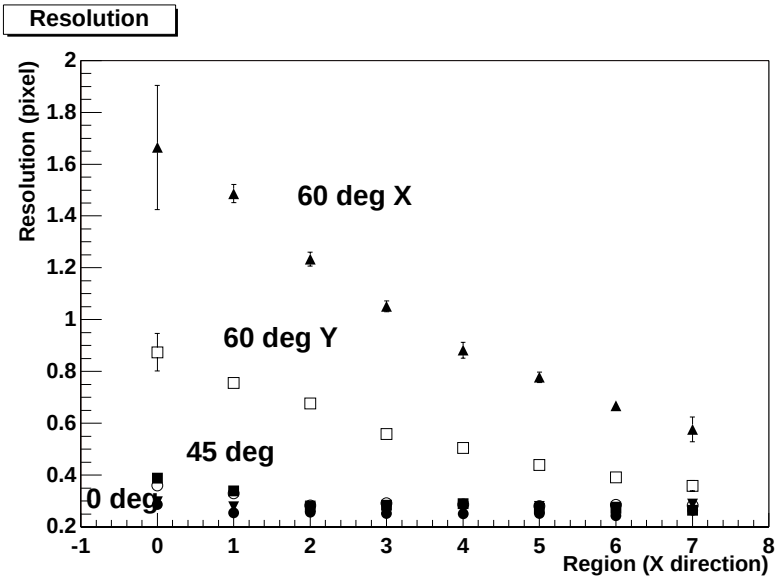

Figure 18: Position dependency of spatial resolution (2GeV/c)

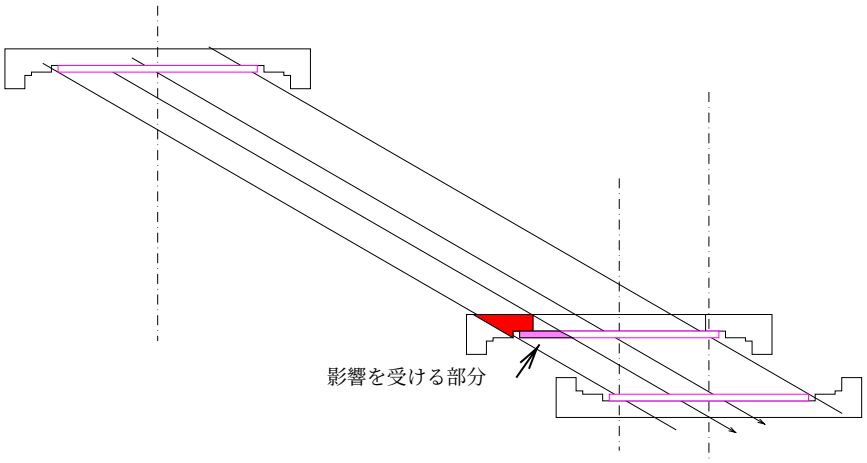

Figure 19: The tracks scattered by the ceramics package

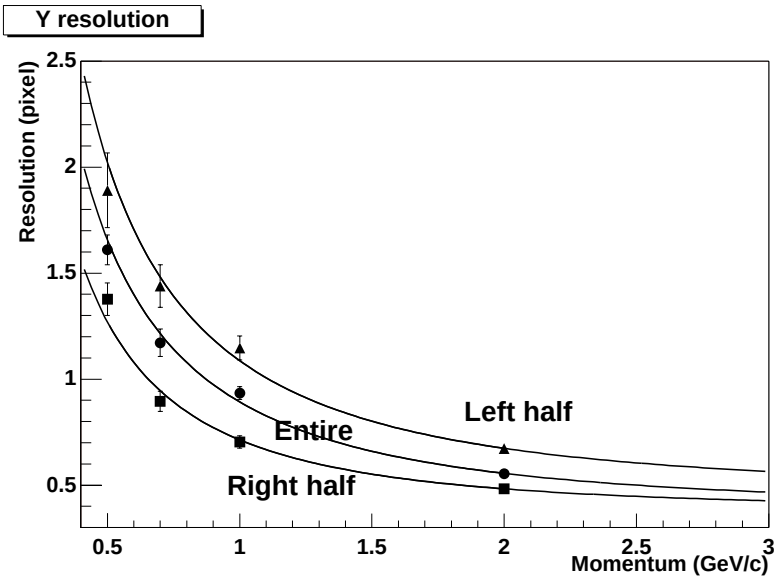

Figure 20: Spatial resolutions with the tracks passing left half, right half, and all tracks

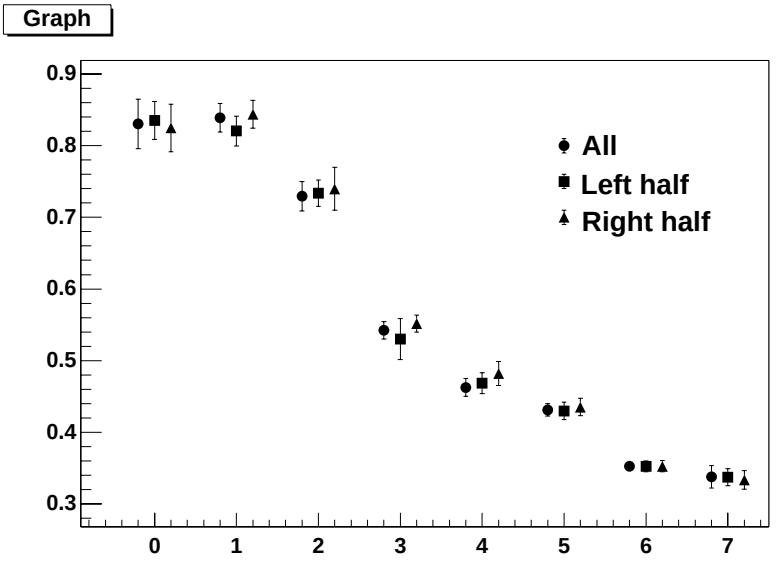

Figure 21: Spatial resolution with left half tracks, right half tracks and all of them

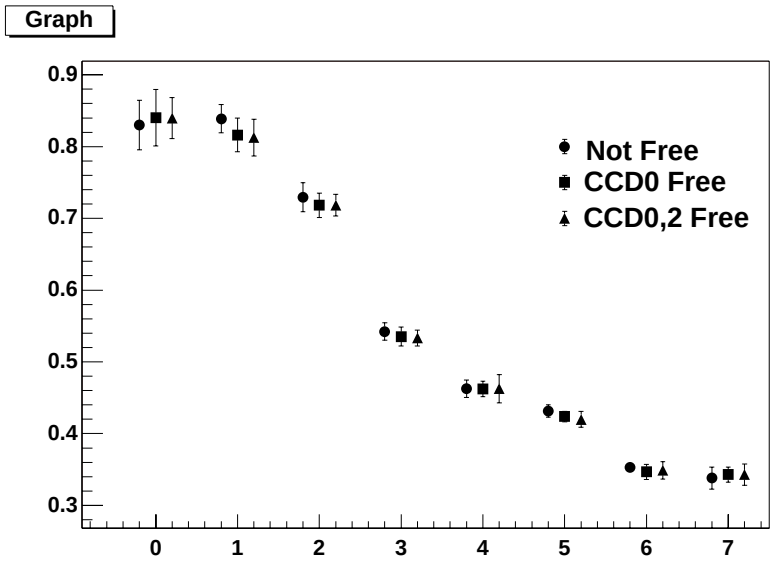

Figure 22: Freeing the center of rotation for CCD0 and CCD2

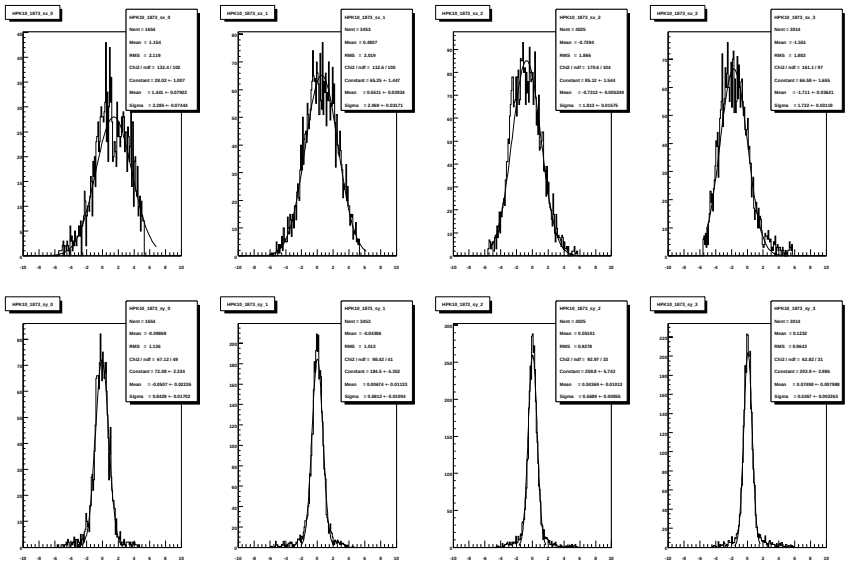

Figure 23: Without tilt consideration, but X dependency remains